An experimental investigation into malachite green degradation using highly active $NiFe_2O_4/Bi_4O_5I_2$ photocatalyst under visible light

Xuet-Wei Woon[1], *Sze-Mun* Lam[1*], *Abdul Rahman* Mohamed[2], and *Honghu* Zeng[3]

[1]Faculty of Engineering and Green Technology, Universiti Tunku Abdul Rahman, Jalan Universiti, Bandar Barat, 31900 Kampar, Perak, Malaysia
[2]School of Chemical Engineering, Universiti Sains Malaysia, Engineering Campus, 14300 Nibong Tebal, Pulau Pinang, Malaysia
[3]College of Environmental Science and Engineering, Guilin University of Technology, Guilin 541004, China

Abstract. In this study, a highly efficient $NiFe_2O_4/Bi_4O_5I_2$ (NFO/BOI) photocatalyst has been successfully synthesized through the two-step hydrothermal method. Various characterization techniques, including X-ray diffraction (XRD), field-emission scanning electron microscopy (FESEM), ultraviolet-visible diffuse reflectance spectroscopy (UV-Vis DRS), and Mott-Schottky (M-S) analysis were employed to scrutinize the physical, chemical, optical, and electrical characteristics of the as-synthesized photocatalyst. The photocatalytic performance of NFO/BOI was assessed through the degradation of malachite green (MG). The findings revealed that both the weight percent of $NiFe_2O_4$ loaded and catalyst loading significantly influenced the degradation efficiency of NFO/BOI on MG. Under 1 hour of visible light irradiation, MG achieved an impressive removal rate of 95.04% using NFO/BOI as the catalyst. Radical trapping experiment confirmed that superoxide anion radical plays a pivotal role in the MG degradation progress. This work introduces a novel direction for designing efficient catalysts for the treatment of water pollution using visible light.

1 Introduction

Since the Industrial Revolution, the cadence of industrialization and urbanization has accelerated global economic growth but also sparked various environmental issues. The widespread use and improper disposal of industrial substances, such as antibiotics and dyes, have led to significant water pollution. Even trace amounts of dyes in water can reduce oxygen levels, disrupting the food chain and harming aquatic ecosystems and human health. [1]. Malachite green (MG), a cationic N-methyl-di-amino-triphenyl-methane dye known for its effectiveness as a biocide in aquaculture, poses significant hazards due to its high toxicity and carcinogenicity to mammalian cells. The detrimental impacts, including mutagenesis, carcinogenesis, and damage to various organs, underscore the need for a comprehensive

*Corresponding author: lamsm@utar.edu.my

evaluation of methods to separate and prevent the discharge of such dyes into water bodies. Various technologies such as coagulation and sedimentation, physical adsorption, advanced oxidation process, Fenton, membrane filtration, and biological elimination have been utilized for dye treatment. Among these techniques, photocatalysis emerges as the optimal choice due to its ability to degrade complex organic compounds into less harmful substances, its environmental friendliness, minimal cost, high stability, and efficient utilization of abundant light energy [2].

As a semiconductor material, $NiFe_2O_4$ possesses a cubic spinel structure and exhibits magnetic properties. Its advantages over other semiconductors include a narrow band gap (1.5 – 1.88 eV), broad visible absorption range, and robust photochemical stability. However, its narrow band gap arrangement leads to the facile recombination of charge carriers, limiting its application in photocatalysis. Various techniques, including micro-emulsion, hydrothermal, sono-chemical, microwave, sol-gel, co-precipitation, mechanical alloying, combustion, and citrate precursor methods, have been employed for synthesizing ferrite materials. Among these, the hydrothermal method stands out as an economical approach, producing ultrafine materials with controlled particle size and morphology at high reaction rates under different temperature and pressure conditions [3]. Furthermore, recent studies on bismuth oxyhalide semiconductors (BiOX) highlight their distinctive crystal structure, favorable electron-hole separation, yet challenges like low carrier separation efficiency, weak redox ability, and limited visible light usage hinder widespread application [4]. Therefore, the creation of a heterojunction by combining two materials with disparate band gaps becomes essential to significantly prolong the lifetime of charge carriers.

In this work, $NiFe_2O_4/Bi_4O_5I_2$ photocatalyst was fabricated using a two-step hydrothermal method. The as-synthesized photocatalyst was characterized through X-ray diffraction (XRD), field-emission scanning electron microscopy (FESEM), ultraviolet-visible diffuse reflectance spectroscopy (UV-Vis DRS), and Mott-Schottky (M-S) analysis to elucidate the physical, chemical, optical, and electrical characteristics. The photocatalytic performance of $NiFe_2O_4/Bi_4O_5I_2$ photocatalyst was evaluated by photodegradation of MG under visible light irradiation. Moreover, the possible mechanism underlying the MG photodegradation process is proposed.

2 Experimental Procedure

All chemicals and reagents used in this experiment are of analytical grade and were used as acquired without any modifications.

2.1 Material synthesis

The $NiFe_2O_4/Bi_4O_5I_2$ photocatalyst was synthesized via a two-step hydrothermal method. Firstly, the $Ni(NO_3)_2{\cdot}6H_2O$ and $Fe(NO_3)_3{\cdot}9H_2O$ with a molar ratio of 1:2 were dissolved in 75 mL deionized water and kept stirring for 30 min. The pH of the suspension was adjusted to 12 via 2 M NaOH. The solution was transferred into a 100 mL Teflon-lined stainless-steel autoclave and heated at 180 °C for 15 h. After cooled, the precipitate collected was centrifuged and rinsed thoroughly with deionized water and ethanol several times. The precipitate denoted as $NiFe_2O_4$ was dried in oven at 80 °C for 12 h and grinded.

Subsequently, $Bi(NO_3)_3{\cdot}5H_2O$ and KI with a molar ratio of 2:1 were dissolved in separate containers with 20 mL deionized water each to form solution A and solution B respectively. 0.2 g polyvinylpyrrolidone (PVP) were dissolved in solution B. Solution B was then slowly dripped into solution A using burette under magnetic stirring to form solution C. The pH of solution C was adjusted to 11 via 2 M NaOH solution and kept stirring for 30 min. *x* g of

$NiFe_2O_4$ was added to solution C and sonicated (x = mass of ratio 2.5%, 5%, 10%, 15%, 20%). The well-mixed solution was transferred into a 100 mL Teflon-lined stainless-steel autoclave and heated at 150 °C for 18 h. After cooled, the obtained precipitate was centrifuged and washed thoroughly with deionized water and ethanol several times. The composite was dried in oven at 60 °C for 10 h and grinded which denoted as NFO/BOI.

2.2 Characterization

The crystal structure and the morphology of the prepared photocatalysts was characterized through X-ray diffraction (XRD, Shimadzu-6000) and field emission scanning electron microscopy (FESEM, Jeol JSM-6701F) respectively. The reflectance of samples was obtained by an ultraviolet-visible diffuse reflectance spectroscopy (UV-vis DRS, JASCO V-730) in the range of 200 – 800 nm. The Gamry Interface 1000T potentiostat electrochemical workstation was utilized to record the Mott-Schottky curve. The 105 W compact fluorescent lamp, platinum electrode, Ag/AgCl electrode, and sample-coated fluorine tin-doped oxide (FTO) glass were used as light source, counter electrode, reference electrode, and working electrode respectively.

2.3 Photocatalytic degradation experiment

The photocatalytic performance of as-synthesized photocatalysts were evaluated by the degradation rate of malachite green (MG) solution. 100 mL of MG solution (10 ppm) was poured in a beaker. 0.1 g of photocatalysts was added into the beaker and equilibrated for 30 min in dark to reach adsorption/desorption equilibrium. Thereafter, the mixture was exposed to a 100 W light emitting diode (LED) lamp as the visible light source and allow for photodegradation on a magnetic-stirrer plate for 1 h. Initial and final concentration were obtained by measuring absorbance of supernatant through spectrophotometer at the maximum wavelength of 620 nm for MG. The weight percent of $NiFe_2O_4$ in the composite and the catalyst loading were varied to study their effects on NFO/BOI photocatalytic activity. The recyclability test was performed to evaluate the stability of the photocatalyst. At the end of each cycle, the photocatalyst was recovered and rinsed with deionized water, dried at 60 °C for 10 h and then reused in the next cycles. Radical trapping experiments were conducted to access the reactive species involved in the reaction mechanism. 5 mM of isopropyl alcohol (IPA) and p-benzoquinone (BQ) were introduced into the MG solution to confirm the presence of hydroxyl radicals (•OH) and superoxide anion radicals ($O^{\bullet}_2^-$) respectively. All of the analytical procedures were repeated to obtain average data.

3 Results and discussion

3.1 Characterization of $NiFe_2O_4/Bi_4O_5I_2$ composite

Figure 1(a) shows the XRD spectra of as-synthesized photocatalysts. The XRD diffraction peaks of pure $Bi_4O_5I_2$ are in accordance with the standard peaks of $Bi_4O_5I_2$ monoclinic structure (JCPDS 71-3448). The XRD pattern of $NiFe_2O_4$ is indexed to the cubic spinel $NiFe_2O_4$ phase (JCPDS 54-0964) with peaks at 30.3°, 35.7°, and 53.8° which matched well to (220), (311), and (422) crystal planes respectively [5]. The characteristic diffraction peaks of the 5 wt% NFO/BOI composite are well aligned with those of the pure material.

Figure 1(b-c) illustrate the morphology of the pure and binary photocatalysts with different magnifications. As presented in Figure 1(b), hydrothermally synthesized $Bi_4O_5I_2$ exhibits as nanoflake-assembled ball-like microspheres with the diameter ranging from 4 - 6

μm. Figure 1(c) shows that $NiFe_2O_4$ nanospheres with average size of 50 - 100 nm have attached to the surface of $Bi_4O_5I_2$ nanoflakes. This observation confirms the successful coupling of $NiFe_2O_4$ nanospheres with $Bi_4O_5I_2$ nanoflakes through the hydrothermal process. Notably, a minimal quantity of $NiFe_2O_4$ nanospheres does not significantly impact the morphology of $Bi_4O_5I_2$.

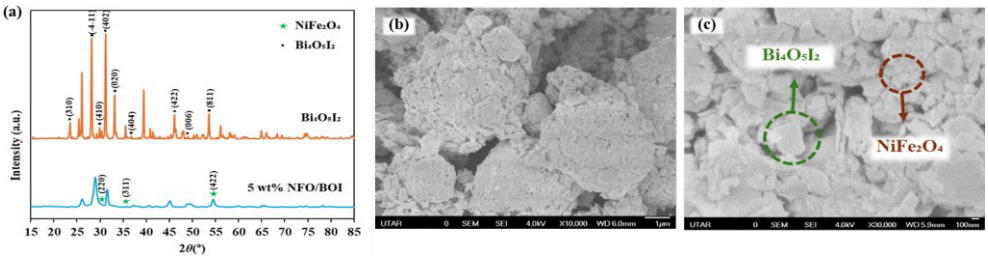

Fig. 1. (a) XRD spectra of $Bi_4O_5I_2$ and 5 wt% NFO/BOI; FESEM images of (b) $Bi_4O_5I_2$, and (c) 5 wt% NFO/BOI.

To further scrutinize the optical characteristics of the synthesized pure and binary photocatalysts, UV-vis DRS spectroscopy was employed, utilizing the Kubelka-Munk (K-M) function to ascertain the band gap energies of pure $NiFe_2O_4$, $Bi_4O_5I_2$, and 5 wt% NFO/BOI composite. Figure 2(a) illustrates the reflectance data of $NiFe_2O_4$ with reflectance edge at 350 nm. Blue shift was observed on the 5 wt% NFO/BOI as compared to pure $Bi_4O_5I_2$ which implies that band gap may be reduced. Based on K-M function, the direct band gap of each material can be obtained by plotting $[F(R)hv]^2$ versus the photon energy [6]. The band gap (E_g) calculated through K-M plots for $NiFe_2O_4$, $Bi_4O_5I_2$, and 5 wt% NFO/BOI was 1.78 eV, 1.7 eV, and 1.55 eV, respectively as shown in Figure 2(b-c).

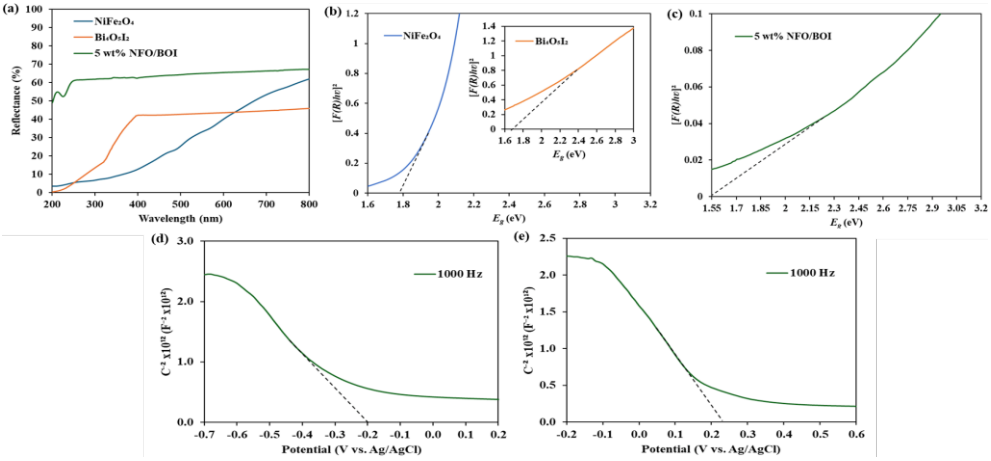

Fig. 2. (a) UV-Vis DRS spectra of $NiFe_2O_4$, $Bi_4O_5I_2$, and 5 wt% NFO/BOI; Kubelka-Munk plots of (b) $NiFe_2O_4$ and (c) 5 wt% NFO/BOI; Mott-Schottky curves at 1000 Hz for (d) $NiFe_2O_4$ and (e) $Bi_4O_5I_2$. Inset: (b) Kubelka-Munk plot of $Bi_4O_5I_2$.

In addition, the valence band energy (E_{VB}) and conduction band energy (E_{CB}) can be calculated by the formulas given below [6].

$$E_{VB} = X - E_0 + 0.5E_g \quad (1)$$

$$E_{CB} = E_{VB} - E_g \quad (2)$$

where X represented the absolute electronegativity and E_0 denoted the energy of free electrons related to hydrogen (4.5 eV). The X obtained from previous studies for $NiFe_2O_4$ and $Bi_4O_5I_2$ are 4.75 eV and 5.93 eV respectively. Therefore, the E_{VB} calculated are 1.14 eV

($NiFe_2O_4$) and 2.28 eV ($Bi_4O_5I_2$) while E_{CB} are –0.64 eV ($NiFe_2O_4$) and 0.58 eV ($Bi_4O_5I_2$). Figure 2(d-e) depict Mott-Schottky (M-S) curves obtained at 1000 Hz for $NiFe_2O_4$ and $Bi_4O_5I_2$. These curves offer information on the flat band potential, aiding in the elucidation of the band structure of the as-synthesized binary photocatalyst. The slope of the Mott-Schottky curves for the pure catalysts are both negative, indicating that $NiFe_2O_4$ and $Bi_4O_5I_2$ are p-type semiconductors with a flat band potential of –0.2 V *vs* Ag/AgCl and 0.23 V *vs* Ag/AgCl, respectively. The measured potential can be converted to -0.003 eV *vs* NHE and 0.427 eV *vs* NHE according to the equation E(NHE) = E(Ag/AgCl) + 0.197 [7].

3.2 Effect of process parameters on photocatalytic activity of $NiFe_2O_4/Bi_4O_5I_2$

The weight percent of $NiFe_2O_4$ loaded in the binary composite is a significant factor affecting the photocatalytic degradation efficiency on MG. As illustrated in Figure 3(a), the removal rate of MG is highest at 95.04% using 5 wt% NFO/BOI for 1 h visible light irradiation. The MG removal rate increased slightly with increased weight percent of $NiFe_2O_4$ from 2.5% to 5% but experienced a drop in the removal rate when the weight percent increase from 5% to 20%, possibly due to the agglomeration of $NiFe_2O_4$ particles in bulk induced by their magnetic properties which lead to uneven loading. The phenomenon implies that only appropriate amount of $NiFe_2O_4$ loaded will improve the photocatalytic activity of the binary composite. The best catalyst 5 wt% NFO/BOI contributed to approximately 50% dark adsorption equilibrium indicating its peculiar morphology for MG adsorption (data not shown). In the following experiments, 5 wt% NFO/BOI was utilized.

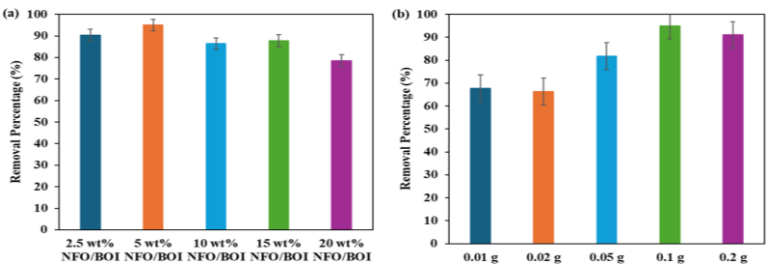

Fig. 3. Effect of (a) $NiFe_2O_4$ loaded wt% and (b) catalyst loading on MG photodegradation.

Figure 3(b) shows the MG removal rate increased when the catalyst loading rises from 0.01 g to 0.1 g then slightly decreased when it continues to rise to 0.2 g. The removal rate at 0.01 g was very low at approximately 67% which indicates poor degradation of MG due to low number of free radical form in the solution. Catalyst loading of 0.1 g in 100 mL of solution (equivalent to 1 g/L) exhibits a relatively high removal rate for MG at 95.04% which designates more active sites provided by the catalyst for photodegradation processes. In addition, more free radicals are produced by light excitation with higher catalyst loadings. However, this trend is only applicable up to 0.1 g, beyond which the removal of MG experienced a slight decrease with higher loadings. This may be attributed to the occurrence of photocatalyst shielding effects and inefficient light penetration caused by high turbidity with high catalyst loadings. Therefore, the optimum process parameters found in this study for the photocatalytic degradation of MG in 1 h light irradiation was catalyst loading of 0.1 g using 5 wt% NFO/BOI. The MG removal rate using 5 wt% NFO/BOI in this work was excellent compared to various reported studies using other catalysts [1, 2, 8].

3.3 NFO/BOI recyclability test and its photocatalysis mechanism

The recyclability and stability of the 5 wt% NFO/BOI composite was assessed by cycling

experiments. As depicted in Figure 4(a), the removal rate of MG remained nearly constant across three cyclic runs, each with an irradiation time of 1 hour. The removal rate experienced a slight reduction in each cyclic run, possibly attributed to a minor loss of catalyst during the recovery process. Overall, the data indicate that the as-synthesized 5 wt% NFO/BOI exhibits favorable recyclability properties.

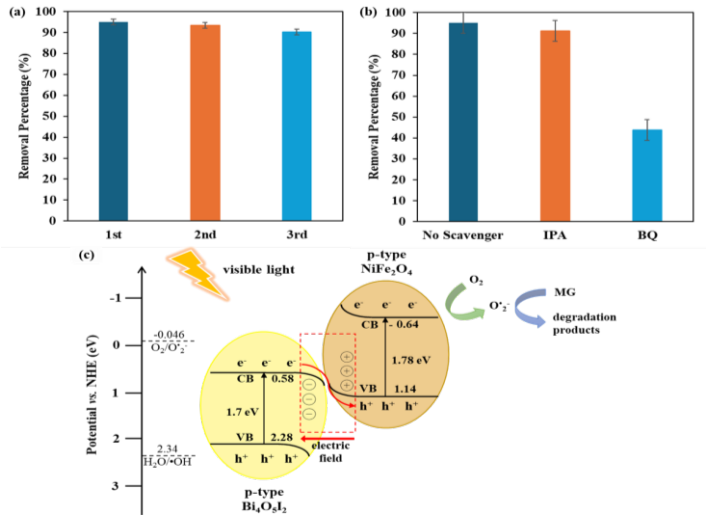

Fig. 4. (a) Cyclic experiment and (b) radical trapping experiment for MG photodegradation under visible light irradiation; (c) Possible photocatalytic degradation mechanism of MG over 5 wt% NFO/BOI.

Radical trapping experiments were conducted to elucidate the free radicals involved in the photodegradation process attacking MG. As shown in Figure 4(b), •OH and $O^{\bullet}_2^-$ were captured using IPA and BQ respectively. The removal rates of MG decreased from 95.04% to 91.26% upon the addition of IPA and to 43.9% with the addition of BQ. These findings indicate that $O^{\bullet}_2^-$ was the primary active species for MG photodegradation utilizing 5 wt% NFO/BOI. The addition of IPA had minimal impact on the MG removal rate, suggesting that •OH did not contribute significantly to the degradation of MG, which was consistent with the results obtained from its band structure. Considering the outcomes of radical trapping experiments and band edge analyses, the possible MG photodegradation mechanism via 5 wt% NFO/BOI was proposed as in Figure 4(c). Photocatalysis, classified as an advanced oxidation process, is initiated through light absorption, inducing the excitation of electrons from the valence band (VB) to the conduction band (CB) in both semiconductors, resulting in the formation of electron-hole (e^-/h^+) pairs. At the contact interface, electrons transfer from $NiFe_2O_4$ to $Bi_4O_5I_2$ due to a variance in Fermi energy levels which initiates the formation of a built-in electric field and induces band bending. Specifically, electrons in CB of $Bi_4O_5I_2$ recombined with holes in the VB of $NiFe_2O_4$ leaving the holes in the VB of $Bi_4O_5I_2$ and electrons in the CB of $NiFe_2O_4$ retained as strong oxidizing and reducing abilities. The $O^{\bullet}_2^-$ from reduced oxygen actively contributed to the photodegradation of MG. The ensuing active species, h^+ and •OH, also exhibit the capacity to oxidize and decompose intricate dye molecules into simpler organic substances [9].

4 Conclusion

In summary, $NiFe_2O_4/Bi_4O_5I_2$ photocatalyst was synthesized through a two-step hydrothermal method. The crystal structure, morphology, optical properties, and electrical

properties of the photocatalysts were investigated using XRD, FESEM, UV-vis DRS, and M-S tests. The photocatalytic performance of the synthesized photocatalyst was evaluated by the photodegradation of MG dye. Evaluation of various process parameters revealed that a catalyst loading of 0.1 g with 5 wt% NFO/BOI achieved the highest removal rate at an impressive 95.04%. Radial scavenging experiments provided additional confirmation, highlighting the major role of $O^{\bullet}_{2}^{-}$ in the photodegradation of MG. Based on the data obtained, the mechanism underlying the photodegradation process was proposed. These noteworthy findings contribute fresh perspectives to the development of an efficient binary composite for photocatalytic degradation in water treatment and environmental pollutant remediation.

This work was supported by the Ministry of Higher Education of Malaysia (MoHE) under the Fundamental Research Grant Scheme (FRGS/1/2022/TK08/UTAR/02/5).

References

1. A. Vijeata, G.R. Chaudhary, S. Chaudhary, A. Umar, Biogenic synthesis of highly fluorescent carbon dots using *Azadirachta indica* leaves: an eco-friendly approach with enhanced photocatalytic degradation efficiency towards malachite green. Chemosphere **341**, 139946 (2023). https://doi.org/10.1016/j.chemosphere.2023.139946
2. K. Mathekga, N.C. Hintsho-Mbita, Synthesis of C. Benghanlensis NiO NPs for the degradation of malachite green and the removal of bacteria. Chem. Phy. Impact **7**, 100277 (2023). https://doi.org/10.1016/j.chphi.2023.100277
3. F. Majid, J. Rauf, S. Ata, I. Bibi, A. Malik, S.M. Ibrahim, A. Ali, M. Iqbal, Synthesis and characterization of $NiFe_2O_4$ ferrite: sol–gel and hydrothermal synthesis routes effect on magnetic, structural and dielectric characteristics. Mater. Chem. Phys. **258**, 123888 (2021). https://doi.org/10.1016/j.matchemphys.2020.123888
4. P. Dhiman, J. Sharma, A. Kumar, G. Sharma, E.A. Dawi, Photocatalytic degradation of malachite green by waste derived bio-char impregnated Bi_5O_7Br/Fe_3O_4 magnetic composite. Opt. Mater. 114568 (2023). https://doi.org/10.1016/j.optmat.2023.114568
5. S.M. Lam, M.K. Choong, J.C. Sin, H.H. Zeng, L.L. Huang, L. Hua, H.X. Li, Z.H. Jaffari, K.H. Cho, Construction of delaminated $Ti_3C_2MXene/NiFe_2O_4/V_2O_5$ ternary composites for expeditious pollutant degradation and bactericidal property. J. Environ. Chem. Eng. **10**, 108284 (2022). https://doi.org/10.1016/j.jece.2022.108284
6. D.S. Ahmed, M. Al-Baidhani, H. Adil, M. Bufaroosha, A.A. Rashad, K. Zainulabdeen, E. Yousif, Recent study of PF/ZnO nanocomposites: synthesis, characterization and optical properties. Mater. Sci. Energy Technol. **6**, 29-34 (2023). https://doi.org/10.1016/j.mset.2022.11.004
7. P.H. Palharim, M.C.D. Caira, C. Gusmão, B. Ramos, A.G.d. Câmara, J.G.A. Pacheco, O.Jr. Rodrigues, A.C.S.C. Teixeira, Enhanced photocatalytic activity and stability of WO_3-AgCl/Ag composites: surface modulation by structure-directing agents for effective sunlight treatment of pharmaceutical wastewater. J. Photochem. Photobiol. A. Chem. **450**, 115433 (2023). https://doi.org/10.1016/j.jphotochem.2023.115433
8. A. Imessaoudene, O. Mechraoui, B. Aberkane, A. Benabbas, A. Manseri, Y. Moussaoui, J.C. Bollinger, A. Amrane, A. Zoukel, L. Mouni, Synthesis of a TiO_2/zeolite composite: evaluation of adsorption-photodegradation synergy for the removal of malachite green. Nano-Structures Nano-Objects **38**, 101191 (2024)
9. Z. Ma, N. Wang, W. Guo, K. Zhang, J. Li, Synthesis of $Bi_4O_5I_2$ for bacterial inactivation with visible light exposure. Mater. Lett. **352**, 135207 (2023). https://doi.org/10.1016/j.matlet.2023.135207